

Wet Disc Contraction to Galactic Blue Nuggets and Quenching to Red Nuggets

A. Dekel¹, A. Burkert²

¹ *Center for Astrophysics and Planetary Science, Racah Institute of Physics, The Hebrew University, Jerusalem 91904 Israel (avishai.dekel@mail.huji.ac.il)*

² *Universitaets-Sternwarte Scheinerstr. 1, Munchen, D-81679, Germany and Max-Planck-Institut fuer Extraterrestrischen Physik, P.O. Box 1312, D-81679 Muenchen, Germany, Max-Planck-Fellow (burkert@usm.lmu.de)*

28 August 2018

ABSTRACT

We study the origin of high-redshift, compact, quenched spheroids (red nuggets) through the dissipative shrinkage of gaseous discs into compact star-forming systems (blue nuggets). The discs, fed by cold streams, undergo violent disc instability (VDI) that drives gas into the centre (along with mergers). The inflow is dissipative when its timescale is shorter than the star formation timescale. This implies a threshold of ~ 0.28 in the cold-to-total mass ratio within the disc radius. For the typical gas fraction ~ 0.5 at $z \sim 2$, this threshold is traced back to a maximum spin parameter of ~ 0.05 , implying that \sim half the star-forming galaxies contract to blue nuggets, while the rest form extended stellar discs. Thus, the surface density of blue galaxies is expected to be bimodal about $\sim 10^9 M_\odot \text{ kpc}^{-2}$, slightly increasing with mass. Blue nuggets are expected to be rare at low z when the gas fraction is low. The blue nuggets quench to red nuggets by complementary internal and external mechanisms. Internal quenching by a compact bulge, in a fast mode and especially at high z , may involve starbursts, stellar and AGN feedback, or Q-quenching. Quenching due to hot-medium haloes above $10^{12} M_\odot$ provides maintenance and a slower mode at low redshift. These predictions are confirmed in simulations and are consistent with observations at $z=0-3$.

Key words: cosmology — galaxies: elliptical — galaxies: evolution — galaxies: formation — galaxies: kinematics and dynamics — galaxies: spiral

1 INTRODUCTION

Observations indicate that a significant fraction of the massive galaxies at redshifts $z = 2 - 3$ are compact ellipticals with suppressed star formation rates (SFR), for which we adopt the nickname “red nuggets” (van Dokkum et al. 2008; Damjanov et al. 2009; van Dokkum, Kriek & Franx 2009; Newman et al. 2010; Damjanov et al. 2011; Whitaker et al. 2012). While the massive star-forming discs of stellar mass $\sim 10^{11} M_\odot$ extend to effective radii of several kpc (Genzel et al. 2006, 2008), the quenched spheroids of a similar mass have effective radii of order 1 kpc. The disc sizes are roughly consistent with the straightforward theoretical expectations based on gas infall through the dark-matter haloes into rotating discs while conserving angular-momentum (Mo, Mao & White 1998; Bullock et al. 2001). Since stellar systems tend to conserve energy and angular momentum, further contraction to form the compact nuggets would require further loss of energy and loss

of angular momentum, which cannot be easily achieved by stellar systems. Thus, the formation of nuggets is likely to be a dissipative process, namely associated with gas inflow into the central regions of the galaxies. Gas inflow is expected to be generated naturally at high redshift, where the gas fraction in the discs is high to begin with (Daddi et al. 2010; Tacconi et al. 2010, 2013). Indeed, there are indicative observational identifications of the progenitors of the red nuggets in the form of “blue nuggets”, which are compact, star-forming galaxies with consistent abundances (Barro et al. 2013a; Williams et al. 2013; Barro et al. 2013b, Bruce et al. in preparation), though the observed abundances of blue nuggets depend on their lifetimes, which could be rather short, depending on the galaxy properties and on the actual quenching mechanism (see below).

The chain of events envisioned at high redshift consists of (1) accretion-driven violent disc instability, (2) dissipative contraction into compact, star-forming blue

nuggets, and (3) quenching of star formation into compact quenched red nuggets. This may be followed by (4) a gradual expansion of the ellipticals.

In phase (1), streams from the cosmic web, consisting of smooth gas and merging galaxies, continuously feed the discs (Birnboim & Dekel 2003; Kereš et al. 2005; Dekel & Birnboim 2006; Ocvirk, Pichon & Teyssier 2008; Kereš et al. 2009; Dekel et al. 2009). The detailed thermal history of the streams in the inner halo (Ceverino, Dekel & Bournaud 2010; Nelson et al. 2013) does not make a difference, as long as the discs are fed with cold gas at the levels consistent with the observed high SFR and gas fraction. The high gas fraction induces VDI, which is characterized by turbulence and perturbations in the form of large transient features and giant clumps (Noguchi 1999; Immeli et al. 2004b,a; Genzel et al. 2006; Bournaud, Elmegreen & Elmegreen 2007; Genzel et al. 2008; Dekel, Sari & Ceverino 2009; Agertz, Teyssier & Moore 2009; Ceverino, Dekel & Bournaud 2010; Ceverino et al. 2012).

In phase (2), dissipative gas inflows into the disc centres are naturally driven by the VDI (Gammie 2001; Dekel, Sari & Ceverino 2009; Krumholz & Burkert 2010; Burkert et al. 2010; Bournaud et al. 2011b; Forbes, Krumholz & Burkert 2012; Cacciato, Dekel & Genel 2012; Elmegreen, Zhang & Hunter 2012; Forbes et al. 2013; Dekel et al. 2013). Similar gas inflows are generated by wet mergers (e.g. Barnes & Hernquist 1991; Mihos & Hernquist 1996; Hopkins et al. 2006). The gas inflows within the discs produce massive compact gas-rich central systems that form stars at a high rate — the blue nuggets. The evolution along the blue sequence of star-forming galaxies is accompanied by gradual stellar and halo mass growth.

The quenching to red nuggets in phase (3) can be driven by two complementary types of mechanisms, bulge quenching and halo quenching. Bulge quenching may involve, for example, starbursts, stellar feedback (e.g. Dekel & Silk 1986; Murray, Quataert & Thompson 2005), AGN feedback (e.g. Ciotti & Ostriker 2007; Cattaneo et al. 2009, for a review), or morphological quenching (Martig et al. 2009). These processes typically operate in a fast mode that may be the dominant trigger for quenching at high redshift. The massive halo quenching may involve, for example, virial shock heating (Birnboim & Dekel 2003; Kereš et al. 2005; Dekel & Birnboim 2006; Kereš et al. 2009), gravitational infall heating (Dekel & Birnboim 2008; Khochfar & Ostriker 2008), or AGN feedback coupled to the hot halo (Dekel & Birnboim 2006; Cattaneo et al. 2009; Fabian 2012). These processes typically operate in a slow, maintenance mode that is dominant at low redshift or at the late stages of the quenching.

Finally, in phase (4), the red nuggets gradually grow in mass and expand by dry mergers along the red sequence.

Here we focus on phase (2), the formation of blue nuggets by VDI-driven wet inflow. Gas inflow that is triggered by wet mergers has been studied before (Hopkins et al. 2006, and references therein). However, it is becoming evident that at high redshift more gas is

driven into the bulge by VDI inflow than by mergers, both based on observations (e.g. Genzel et al. 2006, 2008; Bournaud et al. 2008; Kaviraj et al. 2013b) and on theory including simulations (e.g. Dekel et al. 2009; Bournaud & Elmegreen 2009; Cattaneo et al. 2013; Dekel et al. 2013).

A key idea is that for the inflow within the disc to be intense and dissipative, the characteristic timescale for star formation, t_{sfr} , should be longer than the timescale for inflow, t_{inf} . Otherwise, most of the disc mass will turn into stars before it reaches the bulge, the inflow rate will be suppressed, and the system will become an extended stellar disc. We thus define a “wetness” parameter

$$w \equiv \frac{t_{\text{sfr}}}{t_{\text{inf}}}, \quad (1)$$

such that the condition for a wet inflow is $w > 1$.

Once $w > 1$, we will argue that the contraction continues till the system becomes dispersion dominated and the VDI phases out. A general consequence is that the star-forming galaxies are expected to show a bimodality in central density, separating the extended discs from the compact spheroids.

We will also discuss the predicted distinction between fast and slow modes of contraction and quenching, which originate from VDI discs with $w \gg 1$ and $w \gtrsim 1$ respectively.

At a given mass and redshift, the distribution of w values, and the subsequent variation in evolution path, may be dominated by variations in contraction factor from the virial radius to the disc radius, which can be traced back to variations in spin parameter of the baryons that make the disc. The threshold $w = 1$ can be translated to a critical value of spin parameter, $\lambda_{w=1}$. The fraction of star-forming galaxies that will become blue nuggets then depends on the value of $\lambda_{w=1}$ with respect to the average value of the spin distribution, $\langle \lambda \rangle \sim 0.05$, and it will be computed.

A strong redshift dependence of the blue-nugget fraction is expected due to the variation of gas fraction with redshift. The critical value of central surface density will be estimated as a function of redshift and mass based on scaling relations for gas fraction and stellar-mass fraction in haloes as estimated from observations.

In §2 we derive the threshold condition for wet inflow in terms of the properties that characterize the VDI phase. In §3 we relate this threshold to the spin parameter and its distribution, and estimate the redshift and mass dependence of the fraction of blue nuggets and the surface-density threshold. In §4 we address the possible quenching mechanisms from blue nuggets to red nuggets. In §5 we summarize our conclusions and discuss them.

2 VDI-DRIVEN WET INFLOW

2.1 Violent Disk Instability

We summarize here the basic features of Toomre insta-

bility in a cosmological context following the analysis and notation of Dekel, Sari & Ceverino (2009). Galactic discs at high redshift are expected to develop a gravitational disc instability with a Toomre instability parameter Q smaller than unity (Toomre 1964). The Toomre parameter can be expressed as

$$Q \simeq \frac{\sqrt{2}\Omega\sigma}{\pi G\Sigma} \simeq \frac{\sqrt{2}}{\delta} \frac{\sigma}{V}. \quad (2)$$

The radial velocity dispersion σ and the surface density Σ refer to the cold component of the disc that participates in the disc instability. We sometimes refer to it as “gas”, but it also includes the “cold” young stars. The velocity dispersion σ represents supersonic turbulence that provides the pressure while thermal pressure is negligible. The angular velocity Ω and circular velocity V refer to the characteristic disc radius R_d , $V = \Omega R_d$. The constant $\sqrt{2}$ refers to a flat rotation curve (it stands for $\sqrt{2(1+\nu)}$ where the rotation curve is $V(r) \propto r^\nu$). The cold mass fraction δ is the ratio of mass in the cold component to the total mass within R_d , including gas, young and old stars, and dark matter,

$$\delta \equiv \frac{M_{\text{cold}}}{M_{\text{tot}}}. \quad (3)$$

This is the key physical parameter governing the instability.

The instability in high-redshift galaxies is driven by the high cold surface density that reflects the high mean cosmological density, the high gas accretion rate, and the inability of the star formation rate (SFR) to catch up with the accretion rate. We term this phase *violent disc instability* (VDI) because the associated dynamical processes occur on a galactic orbital timescale, as opposed to the secular evolution at low redshift (see below). The unstable disc tends to self-regulate itself in marginal instability with $Q \simeq 1$.¹ Then eq. (2) implies

$$\delta \simeq \sqrt{2} \frac{\sigma}{V}, \quad (4)$$

so σ/V can replace δ as the variable governing the VDI.

The typical radius and mass of the giant clumps formed by the instability in a disc with respect to the corresponding disc global properties are

$$\frac{R_{\text{clump}}}{R_d} \simeq \frac{\pi}{4} \delta, \quad \frac{M_{\text{clump}}}{M_{\text{cold}}} \simeq \frac{\pi^2}{16} \delta^2. \quad (5)$$

If δ has a systematic dependence on redshift or galactic mass, the clump mass relative to the disc mass will show correlations with these parameters accordingly.

2.2 Inflow within the Disk

The turbulence tends to decay on a timescale comparable to the disc dynamical time (e.g. Mac Low 1999), so it should be continuously powered by an energy source that could stir up turbulence and maintain σ at the level

required for $Q \simeq 1$. In the perturbed disc, which consists of extended transient features and massive compact clumps, gravitational torques drive angular momentum out and cause mass inflow towards the centre, partly as clump migration (Noguchi 1999; Bournaud, Elmegreen & Elmegreen 2007; Dekel, Sari & Ceverino 2009) and partly as off-clump inflow (Gammie 2001; Dekel, Sari & Ceverino 2009; Bournaud et al. 2011b). This inflow down the potential gradient from the disc outskirts to its centre in turn provides the required energy for maintaining $Q \simeq 1$ (Krumholz & Burkert 2010; Burkert et al. 2010; Forbes, Krumholz & Burkert 2012; Cacciato, Dekel & Genel 2012; Forbes et al. 2013). The gas inflow rate $\dot{M}_{g,\text{in}}$ can be estimated by equating this energy gain and the dissipative losses of the turbulence (Dekel et al. 2013),

$$\dot{M}_{g,\text{in}} V^2 \simeq \frac{M_g \sigma^2}{\gamma t_d}. \quad (6)$$

The turbulence decay timescale is the ratio of disc height to velocity dispersion, which for $Q \sim 1$ can be expressed as $\gamma_{\text{dis}} t_d$, where $t_d \equiv R_d/V$ is the global dynamical disc crossing time at the effective radius of the disc, and γ_{dis} is a parameter of order unity. We can think of the parameter γ as a product of three parameters, $\gamma = (2/3)\gamma_g^{-1}\gamma_\Phi\gamma_{\text{dis}}$, where γ_g is the fraction of gas in the inflowing mass, and $\gamma_\Phi V^2$ is the energy gain per unit mass when contracting from the disc radius to the centre. The value of γ is thus of order unity, and it could be as large as a few. We thus obtain for the inflow timescale

$$t_{\text{inf}} = \frac{M_g}{\dot{M}_{g,\text{in}}} \simeq 2\gamma t_d \delta^{-2}. \quad (7)$$

Note that δ refers to the whole cold component, including gas and young stars, while M_g and $\dot{M}_{g,\text{in}}$ refer to the gas only.

Independent estimates based on the mechanics of driving the mass inflow by torques yield similar results to within a factor of 2. Examples of such calculations are (a) an estimate of the rate of energy exchange by clump encounters (Dekel, Sari & Ceverino 2009, eqs. 21 and 7), (b) an estimate of the angular-momentum exchange among the transient perturbations in a viscous disc (Gammie 2001; Genzel et al. 2008; Dekel, Sari & Ceverino 2009, eq. 24), and (c) an estimate based on dynamical friction during clump migration.

One should emphasize that the inflow in the disc is a robust feature of the instability, not limited to clump migration. This is seen in zoom-in AMR cosmological simulations (Dekel et al. 2013). It has been argued based on theoretical estimates that the giant clumps survive intact during their migration (Krumholz & Dekel 2010; Dekel & Krumholz 2013), but even if they are disrupted by stellar feedback in less than a migration time, as has been reproduced in simulations with unrealistically strong radiative stellar feedback (Murray, Quataert & Thompson 2010; Genel et al. 2012; Hopkins, Quataert & Murray 2012; Hopkins et al. 2012), inflow at the rate comparable to eq. (7) is still expected (Cacciato, Dekel

¹ For a thick disk $Q \simeq 0.7$ but this is a detail that does not make a difference at the qualitative level of our analysis here.

& Genel 2012; Forbes et al. 2013; Dekel et al. 2013; Bournaud et al. 2013).

As a note of caution, we should mention that the inflow rate might be modified if the turbulence is driven by sources other than the disc’s self gravity. For example, the cosmological streams that feed the disc may drive non-regulated turbulence but only if the streams largely consist of dense clumps that allow strong coupling of the streams with the higher-density disc (Dekel, Sari & Ceverino 2009; Elmegreen & Burkert 2010; Genel, Dekel & Cacciato 2012). Stellar feedback, by supernovae and radiation pressure, may or may not be a major direct driver of the turbulence (Dekel, Sari & Ceverino 2009; Bournaud et al. 2010; Krumholz & Thompson 2013). The lack of correlation between velocity dispersion and star-forming regions is evidence against it (Forster Schreiber et al. 2009; Genzel et al. 2011). However, outflows can help boosting up σ in an indirect way, by lowering the surface density of the remaining gas that is supposed to be stirred up by the given energy source (Genel, Dekel & Cacciato 2012). In the following, we address the most likely but perhaps idealized case where the disc’s self-gravity is the origin of self-regulated VDI, so eq. (7) is valid.

In a cosmological steady state, where there is balance between cosmological accretion, star formation and VDI-driven inflow within the disc, the typical value is expected to be $\delta \sim 0.3$ (Dekel, Sari & Ceverino 2009; Cacciato, Dekel & Genel 2012; Forbes et al. 2013; Dekel et al. 2013). The corresponding kinematic quantity is $\sigma/V \sim 0.2$, as observed (Genzel et al. 2006, 2008). This has been predicted analytically (Dekel, Sari & Ceverino 2009; Cacciato, Dekel & Genel 2012) and confirmed in cosmological simulations (Dekel et al. 2013). Based on eq. (5), this implies that the clumps are giant, with masses of a few percent of the disc mass. The corresponding timescale for inflow in eq. (7) is $\sim 10t_d$, namely 1-2 orbital times at the disc radius, or ~ 250 Myr at $z \sim 2$. This is the motivation for referring to the disc instability at high redshift as “violent”, unlike the secular, slow evolution associated with bar instability and spiral arms in the stellar-dominated discs at low redshift.

2.3 A Critical δ for Wet Inflow

The timescale for star formation in the disc roughly scales with the free-fall time as

$$t_{\text{sfr}} = \epsilon^{-1} t_{\text{ff}}, \quad (8)$$

where the SFR efficiency is $\epsilon \sim 0.02$ (Krumholz, Dekel & McKee 2012, and references therein). Assuming that star formation occurs in regions that are denser than the mean density of baryons in the disc by a factor of a few, we adopt $t_{\text{ff}} \simeq 0.5t_d$.

Combined with eq. (7), we obtain for the wetness parameter

$$w \simeq (4\gamma\epsilon)^{-1} \delta^2. \quad (9)$$

The condition for a wet inflow, $w > 1$, thus defines a

threshold cold fraction for a wet inflow, $\delta > \delta_{w=1}$, with

$$\delta_{w=1} \simeq 0.28 (\gamma \epsilon_{0.02})^{1/2}. \quad (10)$$

It is interesting to note that this threshold is universal — it does not depend systematically on galaxy mass or cosmic time. Also interesting is the similarity between the derived value of $\delta_{w=1}$ and the typical value of $\delta \sim 0.3$ predicted for the cosmological steady state at high redshift, as well as the corresponding average value of $\sigma/V \sim 0.2$ observed.

Note that δ can be expressed as a ratio of surface densities,

$$\delta \simeq \frac{\Sigma_{\text{cold}}}{\Sigma_{\text{cold}} + \Sigma_{\text{hot}}}, \quad (11)$$

so δ is monotonically increasing with Σ_{cold} . We will refer to Σ later, in comparison to observations.

2.4 Bimodality in compactness

Once started wet, the inflow will remain wet as long as it is within a VDI disc. This is because as a given gas mass contracts to a smaller radius, δ within this radius is expected to increase, and so does w according to eq. (9). To see that δ is increasing during gas contraction, recall that it is inversely proportional to $M_{\text{tot}}(r)$, which is monotonically increasing with r . With w growing, the condition for wet inflow becomes even more valid. This implies that, as long as the VDI is valid, the wet shrinkage is a runaway process. The fact that t_d may become smaller at smaller radii scales out, as it affects both t_{sfr} and t_{inf} in a similar way.

This should lead to a bimodality in the surface density of the population of star-forming galaxies. The gas in the discs in which the initial δ is above the threshold value $\delta_{w=1}$ would flow in and make δ increase away from the threshold value. In discs with δ below the threshold there will be only little or no inflow, and no change in surface density, leaving behind an extended stellar-dominated disc. This should generate a gap in the galaxy population just above the threshold value of $\delta_{w=1}$ (or the corresponding surface density, see below).

2.5 Dispersion-dominated bulge

As long as the disc is in a self-regulated VDI at $Q \simeq 1$ it has $\sigma/V \propto \delta$. Therefore, as the gas contracts, and δ increases, σ/V also increases. At some point, when σ/V is of order unity, this is not a disc anymore, the VDI stops, and the system becomes dispersion dominated. In particular, the actual rotation velocity falls below the circular velocity dictated by the potential well (Burkert et al. 2010), and the rotation curve does not rise at small radii to values of several hundred km s^{-1} .

For illustrative purposes, if we crudely approximate the total mass profile in the relevant range as a fixed isothermal sphere, $M_{\text{tot}} \propto r$, we obtain that during the gas contraction $\sigma/V \propto \delta \propto r^{-1}$. Starting with a disc of $\delta \simeq 0.28$, where $\sigma/V \simeq \delta/\sqrt{2} \simeq 0.20$, the contraction would proceed by a factor of 2.5 in radius till reaching

$\sigma/V \simeq 0.5$, after which the system could be considered dispersion dominated, where standard VDI is no more valid. We thus expect a contraction factor of a few between the original gas disc and the compact spheroid, from a typical effective radius of a few kpc to one kpc, with an enhancement of the surface density by a factor of order 10.

3 BLUE NUGGETS AND SPIN

3.1 A Critical spin parameter

Where and when do we expect VDI-driven blue nuggets, namely $\delta > \delta_{w=1}$? First, at high redshift, when δ (and Σ_{cold}) are high because the gas fraction tends to be high ($\sim 50\%$), both observationally (Daddi et al. 2010; Tacconi et al. 2010, 2013) and based on theoretical considerations (e.g. Krumholz & Dekel 2012). Second, in galaxies where the baryonic spin parameter happened to be relatively low, leading to discs with small radii and therefore higher Σ_{cold} and δ . Third, in galaxies where feedback has not removed a significant amount of gas, which are likely to be the more massive galaxies. This is because gas removal lowers δ both by reducing the gas mass and by increasing the effective spin parameter, as the removed gas tends to come from the central regions where the angular momentum is low. One might also consider galaxies where the cosmological accretion rate happened to be higher than average, but the accretion-driven variations in Σ_{cold} (Forbes et al. 2013) are expected to be smaller than the variations due to the spin parameter (Bullock et al. 2001).

We next use a simple toy model to express the basic parameter for VDI, δ (or σ/V), in terms of the gas fraction and the spin parameter. We then use the distribution of spin parameter to evaluate the abundance of blue nuggets and predict observable criteria for them, as a function of redshift and mass.

We define the parameters λ and m_d as the proportionality factors between the disc baryonic mass M_d and effective radius R_d and the virial mass and radius,

$$M_d \equiv m_d M_v, \quad R_d \equiv \lambda R_v. \quad (12)$$

If specific angular momentum j is conserved during galaxy formation, λ approximates (to within a factor of 2) the halo spin parameter, $\lambda_{\text{spin}} = j/(R_v V_v)$ (see §5). According to tidal-torque theory and cosmological simulations, the halo spin parameter is roughly independent of mass and redshift. It averages to $\langle \lambda_{\text{spin}} \rangle \simeq 0.05$, and it is distributed lognormally with a standard deviation of $\simeq 0.5$ in natural log (Bullock et al. 2001). The effective contraction factor from the virial radius to discs as measured in zoom-in hydro cosmological simulations indeed averages to $\langle \lambda \rangle \simeq 0.05$ in the redshift range $z = 1-4$ and for haloes of $M_v \sim 10^{12} M_\odot$ at $z = 2$ (Dekel et al. 2013, Fig. 13). We denote $\lambda_{0.05} \equiv \lambda/0.05$.

The baryon fraction in the disc is a fraction of the cosmological baryonic fraction $f_b \simeq 0.17$, given that some of the gas is in the halo outside the disc and some has been blown away by feedback. As discussed below,

the average value estimated from observations is in the ballpark of $m_d \sim 0.05$. We denote $m_{d,0.05} \equiv m_d/0.05$.

To compute δ at R_d in the forming disc, we use f_c to represent the fraction of cold baryons (gas and young stars) in the total baryonic disc mass,

$$f_c \equiv \frac{M_{\text{cold}}}{M_d}, \quad (13)$$

so, from eq. (12), $M_{\text{cold}}(R_d) = 0.5 f_c m_d M_v$. The value of f_c is comparable to the gas fraction f_g , and may be larger by up to a factor of 2. We denote $f_{c,0.5} \equiv f_c/0.5$.

For illustrative purposes, we appeal again to the toy model where we crudely approximate the total mass profile in the relevant range of radii as an isothermal sphere with a flat circular velocity, namely $M_{\text{tot}}(r) \propto r$. Then, from eq. (12), $M_{\text{tot}}(R_d) = \lambda M_v$. We thus obtain for the relation between δ and λ

$$\delta_\lambda = 0.25 f_{c,0.5} m_{d,0.05} \lambda_{0.05}^{-1}. \quad (14)$$

Note the similarity between the derived typical value $\delta_\lambda \sim 0.25$ for massive galaxies at $z \sim 2$ and the estimated threshold for wet inflow, $\delta_{w=1} \sim 0.28$ of eq. (10). The natural 1σ scatter of λ is roughly from 0.030 to 0.082 (Bullock et al. 2001), corresponding by eq. (14) with $f_{c,0.5} \sim m_{d,0.05} \sim 1$ to $\delta \sim 0.15 - 0.41$, and thus by eq. (9) to a wetness parameter range $w \sim (0.28 - 2.1)(\gamma \epsilon_{0.02})^{-1}$. This implies that the gas-rich galaxies are expected to populate the whole bimodal range from wet inflow into a compact bulge to the formation of an extended stellar disc.

Given the universal lognormal distribution of spin parameter about an average corresponding to $\langle \lambda \rangle \simeq 0.05$ with a standard deviation of $\sigma_{\ln \lambda} \simeq 0.5$, we can evaluate the fraction of star-forming galaxies that produce massive compact bulges with respect to the total number of star-forming galaxies that also includes extended discs, as a function of redshift and mass. By equating δ_λ from eq. (14) with $\delta_{w=1}$ from eq. (10), we determine the threshold λ corresponding to $w = 1$,

$$\lambda_{w=1,0.05} \simeq \Gamma f_{c,0.5} m_{d,0.05}, \quad (15)$$

where

$$\Gamma \equiv 0.89 (\gamma \epsilon_{0.02})^{-1/2} \sim 1. \quad (16)$$

While this expression should properly capture the characteristic value of $\lambda_{w=1}$ and its general monotonic dependence on $f_c m_d$, the actual expression may be somewhat modified according to possible deviations from the toy model assumed, $M_{\text{tot}} \propto r$. From the distribution of λ , the fraction of compact bulges is expected to be about one half for $\lambda_{w=1} = 0.05$, and it should be monotonically increasing with $\lambda_{w=1}$.

3.2 Fraction of Blue Nuggets

Figure 1 shows the fraction of star-forming galaxies that become blue nuggets as a function of $f_c m_{d,0.05} (\gamma \epsilon_{0.02})^{-1/2}$, as obtained by integrating the log-normal distribution of λ from zero to $\lambda_{w=1}$. We read from the figure, assuming $\gamma \simeq \epsilon_{0.02} \simeq m_{d,0.05} \simeq 1$, that

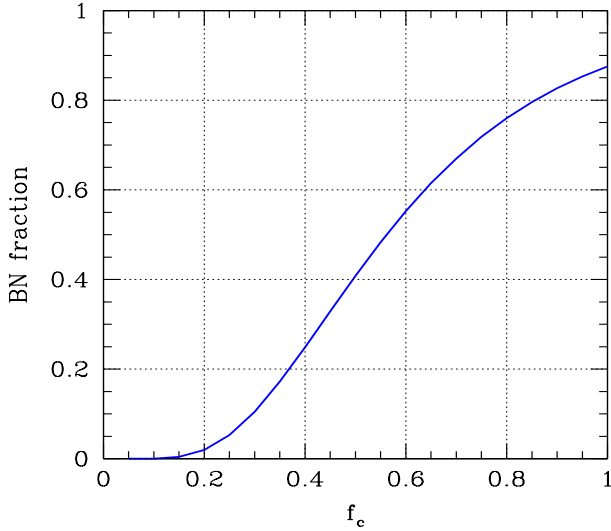


Figure 1. The fraction of star-forming galaxies that become blue nuggets as a function of the fraction of cold mass with respect to the baryon mass, f_c , (comparable to and somewhat larger than the gas fraction f_g). It is obtained from integrating the log-normal distribution of λ from zero to $\lambda_{w=1}$. The parameter f_c in the x axis actually stands for $f_c m_{d,0.05} (\gamma \epsilon_{0.02})^{-1/2}$.

when $f_c \simeq 0.5$ one expects a large blue nugget fraction of ~ 0.4 . For $f_c \simeq 0.2$, the blue-nugget fraction is expected to be drastically reduced to ~ 0.02 , and for $f_c \simeq 0.1$ the blue-nugget fraction is predicted to be only $\sim 3 \times 10^{-4}$.

Since the value of f_c is strongly decreasing with cosmological time (see below), we expect, at any given mass, a significantly higher relative abundance of compact bulges at higher redshifts.

In order to evaluate the mass and redshift dependence of the blue-nugget abundance we should come up with estimates for how the averages of the quantities involved, namely λ , m_d and f_c , scale with mass and redshift. In order to obtain the qualitative behavior, we express these crude estimates as power laws, or scaling relations. While the analysis and results discussed so far could be considered qualitatively robust, the following is naturally less so because the assumed scaling relations are rather uncertain. We focus on the redshift range 1–3 and the halo-mass range from below $10^{11} M_\odot$ to above $10^{12.5} M_\odot$.

For massive haloes, $M_v \geq 10^{12} M_\odot$, we adopt $\langle \lambda \rangle = 0.05$. For less-massive haloes we may write for the disc

$$\langle \lambda \rangle = 0.05 M_{v,12}^{-\ell_m} (1+z)_3^{-\ell_z}, \quad (17)$$

where $M_{v,12} \equiv M_v / 10^{12} M_\odot$ and $(1+z)_3 \equiv (1+z)/3$. The variation with mass and redshift may arise from feedback effects, where the outflows tend to preferentially remove low-spin gas from the galaxy centre and thus increase the effective λ . These effects are expected to be stronger at lower masses and redshift, where the potential wells are shallower (Dekel & Silk 1986). Based on the modeling of Maller & Dekel (2002), one can crudely estimate $\ell_m \sim 1/3$ and $\ell_z > 0$, indicating a weak dependence on mass and redshift.

Based on the observational estimate of molecular gas reported in Tacconi et al. (2013), we crudely estimate

$$f_c \simeq 0.5 M_{v,12}^{-\phi_m} (1+z)_3^{-\phi_z}, \quad (18)$$

with $\phi_m \simeq 1/3$ and $\phi_z \simeq 1$. Indeed, similar scalings with mass and redshift are predicted for the mechanism of metallicity-dependent quenching (Krumholz & Dekel 2012). Then, for the stellar fraction $f_s = 1 - f_c$, near $f_c \sim 0.5$, we can estimate

$$f_s \simeq 0.5 M_{v,12}^{\phi_m} (1+z)_3^{\phi_z}. \quad (19)$$

In order to obtain scaling relations for m_d , we use the Behroozi, Wechsler & Conroy (2013) estimate from observations of M_{star}/M_v as a function of M_v and z . The estimated scaling relation varies depending on the relevant mass range, as M_{star}/M_v reaches a peak near $M_v \sim 10^{12} M_\odot$. We write

$$M_{\text{star}}/M_v \simeq 0.025 M_{v,12}^{\mu_m} (1+z)_3^{\mu_z}, \quad (20)$$

and crudely approximate in two mass ranges

$$\mu_m \simeq \mu_z \simeq \begin{cases} 0, & M_v \sim 10^{11.5-12.5} M_\odot \\ 2/3, & M_v \sim 10^{11.0-12.0} M_\odot. \end{cases} \quad (21)$$

Using $m_d = f_s^{-1} M_{\text{star}}/M_v$ we obtain

$$m_d \simeq 0.05 M_{v,12}^{-\phi_m + \mu_m} (1+z)_3^{\phi_z - \mu_z}. \quad (22)$$

Then, from eqs. (15) and 17,

$$\lambda_{w=1}/\langle \lambda \rangle \simeq \Gamma M_{v,12}^{-2\phi_m + \mu_m + \ell_m} (1+z)_3^{2\phi_z - \mu_z + \ell_z}. \quad (23)$$

With the estimates for the power indices this is

$$\frac{\lambda_{w=1}}{\langle \lambda \rangle} \simeq \begin{cases} \Gamma M_{v,12}^{-1/3} (1+z)_3^2, & M_v \sim 10^{11.5-12.5} M_\odot \\ \Gamma M_{v,12}^{1/3} (1+z)_3^{4/3}, & M_v \sim 10^{11.0-12.0} M_\odot. \end{cases} \quad (24)$$

We see that the critical value of $\lambda_{w=1}$ is strongly increasing with redshift in the whole relevant mass range. This can be translated to a strong redshift dependence of the abundance of blue nuggets among the star-forming galaxies. On the other hand, the predicted mass dependence in eq. (24) is weak. Any mass downsizing in quenching should have another origin, e.g. in a downsizing of the VDI process itself or in halo-mass quenching (see §5).

3.3 A Critical Surface Density

Using eq. (12) we write the stellar surface density within the disc effective radius as

$$\Sigma_s = \frac{0.5 f_s M_d}{\pi R_d^2} = \frac{0.5 f_s m_d}{\pi \lambda^2} \frac{M_v}{R_v^2}. \quad (25)$$

In the Einstein-deSitter cosmological regime, valid to a good approximation at $z > 1$, the virial quantities are related by

$$R_{v,100} \simeq 1.03 M_{v,12}^{1/3} (1+z)_3^{-1}, \quad (26)$$

where $R_{v,100} \equiv R_v/100$ kpc. This gives

$$\Sigma_s \simeq (2\pi)^{-1} \times 10^9 M_\odot \text{ kpc}^{-2} \times \lambda_{0.05}^{-2} f_{s,0.5} m_{d,0.05} M_{v,12}^{1/3} (1+z)_3^2. \quad (27)$$

Using the critical value of $\lambda_{w=1}$ and the scaling relations for f_s and m_d this becomes

$$\Sigma_{s,w=1} \simeq 0.2 \times 10^9 M_\odot \text{ kpc}^{-2} \times M_{v,12}^{4\phi_m - 2\mu_m + 1/3} (1+z)_3^{-4\phi_z + 2\mu_z + 2}. \quad (28)$$

After the dissipative contraction, the spheroid is expected to have contracted by a factor of a few, so the stellar surface density of the compact spheroid is expected to be larger by a factor of ~ 10 . The predicted scaling is thus

$$\Sigma_{s,w=1} \simeq 2 \times 10^9 M_\odot \text{ kpc}^{-2} \times \begin{cases} M_{v,12}^{5/3} (1+z)_3^{-2}, & M_v \sim 10^{11.5-12.5} M_\odot \\ M_{v,12}^{1/3} (1+z)_3^{-3/2}, & M_v \sim 10^{11.0-12.0} M_\odot. \end{cases} \quad (29)$$

While the magnitude of the surface density should be considered as a reliable order-of-magnitude estimate, one should recall that the scalings with mass and redshift are based on uncertain scaling relations for the gas fraction, m_d and λ , and should therefore be considered with a grain of salt.

3.4 Preliminary Comparison to Observations

Our aim in the current paper is to present the key features of the formation of blue nuggets through VDI, and to make qualitative predictions based on an idealized toy model. A detailed comparison of the model to observations is premature; it will have to wait for more quantitative predictions, e.g., based on simulations, and for the proper observations to accumulate and allow detailed analysis and reliable statistical results. Here we briefly comment on the encouraging qualitative consistency between the crude theoretical predictions and the pioneering observational results concerning blue nuggets.

The predicted strong redshift dependence of the fraction of blue nuggets among the star-forming galaxies is indeed seen in the observed samples by Barro et al. (2013a), which contain galaxies of stellar mass $10^{10.5-11.5} M_\odot$ in the redshift range $z = 1 - 3$. In their Figure 8, comparing the blue to the grey histogram, one can see that the blue-nugget fraction drops at a rate consistent with the predicted rate, from $\sim 40\%$ at $z = 2.2 - 2.6$ to $\sim 10\%$ at $z = 1.0 - 1.4$, and to an even smaller value by $z = 0.5 - 1.0$.

The star-forming galaxies at $z > 2$ indeed indicate a “bimodality” in compactness, consisting of a non-negligible population of compact blue nuggets and a large body of star-forming galaxies with low surface-densities, qualitatively consistent with the model predictions. A recent analysis of CANDELS data (van der Wel et al. in preparation) reveals a similar distribution of sizes, as a function of mass and redshift, with the radii spread over a decade in each bin of mass and redshift, from 1 to 10 kpc.

The threshold for blue nuggets as identified by Barro et al. (2013a) at $z \sim 2 - 3$ corresponds to an effective stellar surface density of $\Sigma_s \sim 2.5 \times 10^9 M_\odot \text{ kpc}^{-2}$.

This is derived from their Figure 1 (or Figure 7), using $M_{\text{star}} = 10^{11} M_\odot$ and the corresponding threshold value of $R_d \simeq 2.5 \text{ kpc}$. This observed threshold is consistent with the predicted threshold, eq. (29).

At a redshift somewhat smaller than unity, $z = 0.5 - 0.8$, and in the stellar mass range $10^{10.3-11.3} M_\odot$, Cheung et al. (2012) find a similar threshold for the effective surface density of blue, green and red nuggets at $\Sigma_s \sim 10^9 M_\odot \text{ kpc}^{-2}$ (Figure 5, bottom-left panel). It is also seen as a threshold in the surface density within the inner 1 kpc, $\Sigma_{1 \text{ kpc}} \simeq 2 \times 10^9 M_\odot \text{ kpc}^{-2}$ (Figure 5, bottom-left panel). This is in the ball park of the prediction in eq. (29). These data do show an increase of $\Sigma_{1 \text{ kpc}}$ with mass as predicted (E. Cheung, private communication), though the predicted redshift dependence is not detected.

At low redshift, $z < 0.075$, and in the stellar mass range $10^{9.75-11.25} M_\odot$, Fang et al. (2013) find complementary evidence for blue, green and red nuggets. By plotting the sSFR estimator as a function of $\Sigma_{1 \text{ kpc}}$ in bins of stellar mass one can interpret the distribution of galaxies as tracing evolutionary tracks. For stellar masses in the range $10^{10.5-11.25} M_\odot$, the detected threshold in their Figure 6 is at $\Sigma_{1 \text{ kpc}} \sim 3 \times 10^9 M_\odot \text{ kpc}^{-2}$. The associated value of the effective surface density can be estimated to be a factor of a few smaller. The overall scaling with mass as reported by Fang et al. (2013) is $\Sigma_{1 \text{ kpc}} \propto M_{\text{star}}^{0.6-0.7}$, qualitatively along the lines of the predicted scaling in eq. (29). The predicted increase of $\Sigma_{s,w=1}$ at low redshift is not seen in the data. If the predicted scaling with redshift is valid (reflecting correct adopted scalings of f_c , m_d and λ), the failure to reproduce it may indicate that most of the quenching of galaxies that are now red nuggets actually occurred at higher redshifts.

Indeed, Figure 6 of Fang et al. (2013) indicates downsizing, in the sense that the relative abundance of blue and green nuggets compared to red nuggets is decreasing with mass. This implies that most of the more massive galaxies have quenched in the past while many of the less massive galaxies are quenching right now. The origin of this downsizing may be related to halo quenching (§4.2), or to downsizing in the condition $Q \sim 1$ for VDI.

Independently, based on measurements of cold gas at low redshift, Kauffmann et al. (2012) report a threshold effective surface density for gas-poor galaxies at $\Sigma_s \simeq 10^9 M_\odot \text{ kpc}^{-2}$ for $M_{\text{star}} \sim 10^{11} M_\odot$, with a scaling $\Sigma_s \propto M_{\text{star}}^{0.4}$ (Figures 9 and 10, top-left panels). These are consistent with the findings of Fang et al. (2013), and with the theoretical prediction, eq. (29).

Barro et al. (2013b) have recently studied the structural properties and stellar populations of 45 massive blue nuggets from the CANDELS survey at $z = 2 - 3$, and provided further evidence that these galaxies are consistent with being the descendants of the more extended star-forming discs and the progenitors of the red nuggets at $z \sim 2$. In particular, the indicated contraction factors from discs to blue nuggets, and the more spheroidal morphologies of the latter, are consistent with the model predictions for a contraction factor of a

few and for the system becoming dispersion dominated during the contraction.

4 QUENCHING: BLUE TO RED NUGGETS

The creation of compact, dispersion-dominated blue nuggets allows the development into compact red nuggets of similar structural properties. Furthermore, the high SFR induced by the high gas density provides natural conditions for the subsequent quenching of star formation necessary for the development into passive red nuggets. We provide here a discussion of the possible quenching mechanism, trying to distinguish between internal mechanisms related to the central structure of the galaxies and external mechanisms associated with the circum-galactic medium (CGM) in the dark-matter halo. We then discuss the possible association of these quenching mechanisms with fast and slow evolution modes, both in the quenching and the compactification phases, and connect these modes with the disc wetness parameter and the galaxy spin parameter as introduced in our analysis above.

4.1 Internal Quenching

A compact gas bulge with a high Σ_g naturally gives rise to a central phase of high SFR. This could cause a drastic decrease in Σ_g by gas consumption into stars as well as gas outflow due to stellar feedback, and thus lead to rapid quenching, possibly over ~ 1 Gyr or less. Similarly, the dissipative inflow leads to a rapid growth of the central black hole (Bournaud et al. 2011b), and the quenching could be a result of gas removal by AGN feedback (though perhaps not immediately Gabor & Bournaud 2013).

The development of a compact massive bulge could also lead to quenching by stabilizing the VDI, where the Toomre Q parameter is driven to values above unity. Recalling that $Q \propto \Omega\sigma/\Sigma_{\text{cold}}$, eq. (2), we notice that Q -quenching can happen in three different ways, or in a combined way, as follows:

- Morphological quenching (Martig et al. 2009), where the growth of total central density is expressed as an increase in Ω . There is observational indication for such an effect (Saintonge et al. 2012; Crocker et al. 2012; Fang et al. 2013; Martig et al. 2013), and recent evidence in spectroscopically observed $z \sim 2$ galaxies (Genzel et al. 2013).
- A drop in Σ_g , and thus in Σ_{cold} , by star formation and outflows. In this case the mass gradually becomes dominated by stars, whose velocity dispersion becomes higher than that of the gas, which increases the effective Q further. The consequent shutdown of the VDI-driven inflow makes Σ_g even lower, such that Q rises in a runaway process. This is demonstrated in analytic calculations and one-dimensional simulations (Cacciato, Dekel & Genel 2012; Forbes et al. 2013), where Ω is kept fixed.
- An increase in the gas σ as a result of stellar or

AGN feedback (Krumholz & Thompson 2013), which quenches further star formation.

4.2 Halo Quenching

The observed distribution of galaxies in the plane of specific SFR (sSFR) versus Σ_s has an “L” shape, defined by a star-forming side of varying Σ_s at a high sSFR and a compact side of varying sSFR at a high Σ_s , along which one envisions shrinkage and quenching respectively. In particular, the compact side reveals that a compact galaxy could be either star forming or quenched or in transition between the two (Kauffmann et al. 2012; Cheung et al. 2012; Fang et al. 2013; Barro et al. 2013a). This indicates that the compactness is only a necessary condition for quenching, not sufficient, so a complementary second mechanism is required for quenching. Independently, the shutdown of cold accretion into the halo centre by a hot CGM in the halo is clearly necessary for the long-term maintenance of quenching. Such a halo quenching could be the required second mechanism. A study of SDSS galaxies at low redshift indeed indicates that both compactness and a massive halo are required for a high quenched fraction of galaxies (J. Woo et al. in preparation). This work also indicates that halo quenching is likely to be a slow mode of quenching, lasting a few Gyr, as the cold gas reservoir in the disc is slowly exhausted and the SFR is fading out.

The CGM is likely to be heated by a stable virial shock once the halo grows above a critical mass on the order of $\sim 10^{12} M_\odot$ (Birnboim & Dekel 2003; Kereš et al. 2005; Dekel & Birnboim 2006; Kereš et al. 2009). While at $z > 2$ narrow cold streams penetrate the hot medium and keep the SFR high, at lower redshifts the penetration is halted once the medium has been shock heated. Besides halting the cold streams, the presence of a hot medium improves the coupling between AGN-driven wind and the accreting gas, and thus makes the AGN feedback more effective in quenching the SFR (Dekel & Birnboim 2006).

In even more massive haloes, $M_v \geq 10^{13} M_\odot$, the gravitational power associated with the gas streaming into the halo can provide the heating that compensate for the cooling rate. If the accretion is appropriately clumpy, or if the streams couple to the medium, this gravitational heating can cause proper quenching at the halo centre (Dekel & Birnboim 2008; Khochfar & Ostriker 2008). In addition, the dynamical friction that acts on subhaloes or satellite galaxies as they spiral into the central galaxy extracts energy (and angular momentum) from their orbits and can thus heat up the medium (El-Zant, Kim & Kamionkowski 2004).

4.3 Fast and Slow modes

The relative role of internal quenching and halo quenching may determine whether the quenching is fast or slow. As eluded to above, this can be decided by the degree of wetness in the original disc (which is a function of the galaxy spin parameter).

In the fast mode, a disc that forms with $w \gg 1$ would form stars at a high rate and move quickly along the blue sequence towards larger stellar masses and higher central surface densities. Once the gas central density is high, a rapid starburst would lead to rapid quenching. The galaxies in this fast mode are to be found in the blue side of the blue sequence, and in the high- Σ_s side of the green valley, along the external side of the L-shape track. By the time the galaxy is on the red sequence, the quenching is maintained if the halo is already above the critical mass so the CGM is hot. This fast mode is expected to be dominant once the gas fraction is high, namely preferentially at high redshift.

In the slow mode, a disc that has $w \gtrsim 1$ would form stars in a moderate rate and spend more time on the red sequence, as it slowly evolves toward higher stellar masses and higher central densities. In parallel to slowly developing a compact core, the haloes are growing and becoming massive enough to support a virial shock that causes slow quenching towards the red sequence. The slow-mode galaxies are to be found in the red side of the blue sequence, and then on the low- Σ_s side of the green valley, along an interior L-shape track. The halo masses are expected to be somewhat more massive on the slow-mode track.

Galaxies with $w < 1$ would form stars in a disc over on a long timescale, leaving behind an extended disc. They may remain star forming, like the Milky Way, or eventually quench by the halo when it is sufficiently massive.

4.4 Downsizing in Quenching

While the above analysis of the consequences of wetness does not seem to explicitly predict that more massive galaxies are quenched earlier, there are several other mechanisms that naturally lead to downsizing of quenching (also mentioned in Bournaud et al. 2011b), which we should briefly discuss here for completeness.

First, such a downsizing is a natural prediction of halo quenching (Dekel & Birnboim 2006; Cattaneo et al. 2008), where more massive haloes tend to cross the threshold mass for virial shock heating earlier. In turn, a lower-mass threshold for the onset of star formation helps the massive galaxies form stars early, which by itself leads to downsizing (Neistein, van den Bosch & Dekel 2006; Bouché et al. 2010; Krumholz & Dekel 2012).

Second, there is a natural downsizing in the conditions for VDI, which could translate to downsizing in the formation of blue nuggets, and then red nuggets. The Toomre Q parameter tends to be lower for less massive galaxies, e.g., because of the higher cold gas fraction that is maintained in low-mass galaxies to lower redshifts (e.g. Kannappan 2004; Tacconi et al. 2013). This could be a natural result of stronger non-ejective feedback in low-mass galaxies (Krumholz & Dekel 2012). Another reason for quenching in more massive galaxies is the more efficient growth of bulge-to-disc ratio in more massive galaxies, leading to earlier morphological quenching (Martig et al. 2009).

4.5 Preliminary Comparison to Observations

Evidence for the dominance of a fast quenching mode at high redshifts is provided by the rather rapid appearance of the red sequence during a period shorter than ~ 0.7 Gyr between $z \sim 2.8$ and $z \sim 2.2$ (Barro et al. 2013a, Figure 2). An observational indication for the presence of a minor fast mode of quenching at low redshifts is found in green-valley SDSS galaxies in transition from blue to red (H. Yesuf et al. in preparation). A small fraction of the green-valley galaxies are identified as post-starburst galaxies, which implies that they are quenching rather rapidly, while the rest are quenching more slowly. Indeed, these fast-mode galaxies tend to be of higher surface density and lower halo mass.

An intrinsic difficulty in detecting the fast mode of evolution arises from the fact that the blue-nugget phase with high SFR may be rather short, implying a low observable abundance of blue nuggets. The abundance is expected to be low even if a significant fraction of the star-forming galaxies have shrunk to blue nuggets and most of the red nuggets have passed through this phase, as expected at high redshift. Detecting such galaxies on the blue side of the green valley as post-starburst galaxies may be more feasible.

Studies of the global shapes of $z \sim 2$ red nuggets indicate that they tend to be flattened spheroids, sometimes characterized as “disk-like” or “disk-dominated” (van der Wel et al. 2011; Chang et al. 2013). This is consistent with the idea that the progenitor blue nuggets formed by VDI-driven inflow from rotating discs, and that the subsequent quenching was not associated with a dramatic event that is likely to change the global shape, like a major merger.

5 CONCLUSION AND DISCUSSION

Given that the high-redshift compact ellipticals are likely to have formed by dissipative gas inflow toward the galaxy centre, we investigated the likely main channel for this process at high redshift — the gas contraction naturally associated with VDI. Figure 2 schematically illustrates the main components of the proposed scenario.

Our main conclusions are as follows:

- Given a disc in a VDI phase, a necessary condition for wet inflow is that the timescale for star formation is longer than the timescale for inflow, namely that the wetness parameter, $w = t_{\text{sfr}}/t_{\text{inf}}$, is larger than unity.
- This condition is fulfilled once the cold-to-total mass ratio within the disc radius is above a threshold value $\delta_{w=1} \simeq 0.28$. This happens to be comparable to the value obtained by discs in a cosmological steady state.
- For a cold-to-baryonic mass ratio $f_c \sim 0.5$, and a baryonic fraction within the virial radius of $m_d \sim 0.05$, both being approximately valid at $z \sim 2$, the threshold at $w = 1$ corresponds to a spin parameter of $\lambda_{w=1} \simeq 0.05$, which is near the average spin parameter for haloes. Given the lognormal distribution of spin parameters (Bullock et al. 2001), this implies

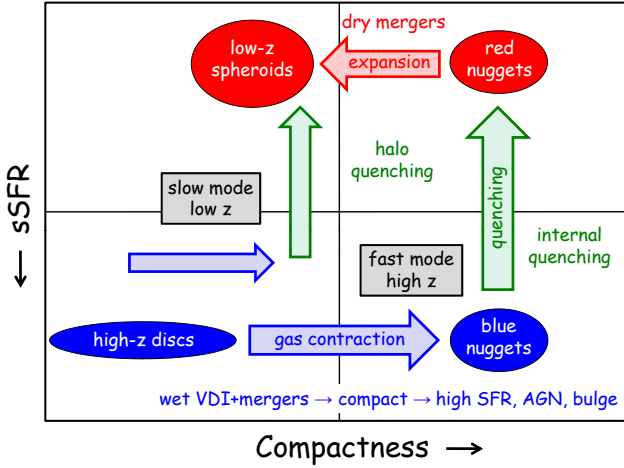


Figure 2. A schematic diagram illustrating the scenario addressed in this paper. The fast mode, likely dominant at high redshift, involves VDI-driven wet gas contraction of the denser high-redshift discs into compact, gaseous, star-forming blue nuggets, followed by quenching into compact, passive, stellar red nuggets. The blue-nugget compactness triggers the quenching by internal processes including stellar and AGN feedback and Q-quenching, to be maintained by hot-halo quenching. The red nuggets eventually de-compactify by dry mergers into the low- z spheroids. A slower mode, potentially dominant at low redshift, may involve medium-wetness discs that contract slowly and possibly quench by halo only, without passing through a blue-nugget phase. High angular momentum galaxies form extended stellar-dominated discs (not illustrated here).

that about one half of the star-forming galaxies are expected to contract to blue nuggets, while the rest form extended stellar discs.

- Blue nuggets are expected to be much less frequent at low redshifts, both relative to the diffuse star-forming galaxies, and the quenched galaxies.
- The star-forming galaxies at high z are expected to show a corresponding bimodality in effective stellar surface density about a value $\Sigma_s \sim 10^9 M_\odot \text{ kpc}^{-2}$. This critical value is expected to be weakly increasing with mass.
- The blue nuggets quench to red nuggets by mechanisms of two types. Internal quenching can be associated with starbursts, stellar or AGN feedback, and Q-quenching. It can serve for triggering the quenching, and may be responsible for a fast transition from blue to red nuggets, especially valid at high redshift. Halo quenching can shut down the accretion onto the galaxy due to virial shock heating or gravitational-infall heating once the halo grows above a critical mass of $\sim 10^{12} M_\odot$. It can serve for maintenance of the quenched phase, and may be responsible for a slow mode of quenching, valid mostly at low redshifts.
- These predictions are largely confirmed in hydro-cosmological simulations (Zolotov et al. in preparation) and are demonstrated using semi-analytic simulations (Porter et al. in preparation). Both show evolutionary tracks similar to those predicted by the toy model and indicated from the observations, where gaseous disks shrink to blue nuggets, which quench to

red nuggets, and then gradually grow in size by dry mergers.

- The predictions are qualitatively consistent with the results obtained from observations of the star-forming and quenched galaxy populations, focusing on the blue and red nuggets at $z < 1$ (Cheung et al. 2012; Kauffmann et al. 2012; Fang et al. 2013) and at $z = 1 - 3$ (Barro et al. 2013a; Kaviraj et al. 2013a,b; Lee et al. 2013; Williams et al. 2013; Barro et al. 2013b, Bruce et al. in preparation).

In the context of the role of the wetness parameter $w = t_{\text{sfr}}/t_{\text{inf}}$ in determining the galaxy type, we recall that early theories of galaxy formation have proposed that the formation of discs and spheroids can be determined by the timescale for star formation with respect to the dynamical time for the galaxy buildup (Larson 1976). However, there the buildup timescale referred to the global infall into the galaxy, while here it is specifically the VDI-driven inflow within the disc. The two timescales are indirectly related, as the cosmological in-streaming is the driver of VDI, which in turn generates the inflow within the disc, but they are not necessarily the same. In particular, the cosmological accretion time at $z > 1$ is proportional to $(1+z)^{-5/2}$ (e.g. Neistein & Dekel 2008; Dekel et al. 2013), while the disc inflow rate is proportional to the dynamical time t_d , which scales like the Hubble time, $t \propto (1+z)^{-3/2}$.

Similarly, the idea that the spin parameter can distinguish between spheroids and discs has been around for a long time (Fall & Efstathiou 1980; Blumenthal et al. 1984; Mo, Mao & White 1998; Dutton et al. 2007). However, this idea had difficulties in the context of the common wisdom that spheroids form by major mergers of discs, which commonly generate high-spin systems. The role of the spin parameter in determining the fate of a galaxy becomes clearer in the context of spheroid formation by VDI.

The estimates of the blue-nugget abundance were based on the assumption that the distribution of specific angular momentum of the baryons is similar to that of the total halo matter. This is only a crude approximation. On one hand, simulations indicate that the specific angular momentum in the incoming baryon streams is higher than that of the dark-matter halo. On the other hand, the baryons exchange angular momentum with the dark matter due to strong torques as they stream in (Pichon et al. 2011; Kimm et al. 2011; Tillson et al. 2012; Codis et al. 2012; Danovich et al. 2012; Stewart et al. 2013, M. Danovich et al. in preparation). The quantitative estimates should therefore be trusted to an accuracy of no more than a factor of 2.

The scenario addressed here predicts the formation of blue nuggets as dispersion-dominated star-forming systems, with $\sigma/V \geq 0.5$. This reminds us of the observed population of dispersion-dominated systems (Law et al. 2012; Newman et al. 2013). However, while the latter tend to be less massive and of lower metallicity, the blue nuggets discussed here could be massive and of relatively high metallicity. It thus seems plausible that there are two types of dispersion-dominated star-forming systems, one that represents the early stages of

evolution of a VDI disc, and the other that arises as a product of VDI — the blue nuggets.

The scenario discussed above also predicts the high-redshift presence of young blue nuggets surrounded by star-forming clumpy discs or rings. There are already possible detections of such cases (Elmegreen, Elmegreen & Ferguson 2005; Bournaud et al. 2011a, Figure 9).

The low-redshift descendants of the red nuggets resulting from blue nuggets that originated from VDI discs are expected to be rotating spheroids. The predicted systems resemble most of the present day elliptical galaxies, which show rapid rotation within their effective radii (Emsellem et al. 2011), dropping to slow rotation velocities at a few effective radii (Romanowsky et al. in preparation). The giant non-rotating ellipticals must have formed by subsequent dry mergers.

Our toy model has not addressed the detailed star formation and stellar evolution during the compactification into blue nuggets and quenching to red nuggets, so we do not attempt here to make quantitative predictions for the abundances of galaxies in the different stages of evolution, or for the detailed properties of the fast and slow modes of evolution. This will be done utilizing cosmological simulations, where mergers also contribute to the evolution, and the evolution of the stellar population, including SFR and feedback, is explicitly followed (e.g. Zolotov et al. in preparation). The simulations will allow comparison of theory to observations of the evolutionary modes at low and especially high redshift, as relevant observations accumulate.

ACKNOWLEDGMENTS

We acknowledge stimulating discussions with Frederic Bournaud, Sandy Faber, David Koo, Reinhard Genzel, Mark Krumholz, Joel Primack, and Joanna Woo. This work was supported by GIF grant G-1052-104.7/2009 and by a DIP grant. The work of AD was supported by ISF grant 24/12, by NSF grant AST-1010033, and by the I-CORE Program of the PBC and The ISF grant 1829/12. AB acknowledges financial support by the Cluster of Excellence “Origin and Structure of the Universe”.

REFERENCES

- Agertz O., Teyssier R., Moore B., 2009, *MNRAS*, 397, L64
- Barnes J. E., Hernquist L. E., 1991, *ApJ*, 370, L65
- Barro G. et al., 2013a, *ApJ*, 765, 104
- Barro G. et al., 2013b, *arXiv:1311.0000*
- Behroozi P. S., Wechsler R. H., Conroy C., 2013, *ApJ*, 762, L31
- Birnboim Y., Dekel A., 2003, *MNRAS*, 345, 349
- Blumenthal G. R., Faber S. M., Primack J. R., Rees M. J., 1984, *Nature*, 311, 517
- Bouché N. et al., 2010, *ApJ*, 718, 1001
- Bournaud F. et al., 2011a, *ApJ*, 730, 4
- Bournaud F. et al., 2008, *A&A*, 486, 741
- Bournaud F., Dekel A., Teyssier R., Cacciato M., Daddi E., Juneau S., Shankar F., 2011b, *ApJ*, 741, L33
- Bournaud F., Elmegreen B. G., 2009, *ApJ*, 694, L158
- Bournaud F., Elmegreen B. G., Elmegreen D. M., 2007, *ApJ*, 670, 237
- Bournaud F., Elmegreen B. G., Teyssier R., Block D. L., Puerari I., 2010, *MNRAS*, 409, 1088
- Bournaud F., Perret V., Renaud F., Dekel A., Elmegreen B. G., Elmegreen D. M., Teyssier R., et al., 2013, *arXiv:1307.7136*
- Bullock J. S., Dekel A., Kolatt T. S., Kravtsov A. V., Klypin A. A., Porciani C., Primack J. R., 2001, *ApJ*, 555, 240
- Burkert A., Genzel R., Bouché N., Cresci G., Khochfar S., Sommer-Larsen J., Sternberg A., et al., 2010, *ApJ*, 725, 2324
- Cacciato M., Dekel A., Genel S., 2012, *MNRAS*, 421, 818
- Cattaneo A., Dekel A., Faber S. M., Guiderdoni B., 2008, *MNRAS*, 389, 567
- Cattaneo A., Faber S. M., Binney J., Dekel A., Kormendy J., Mushotzky R., 2009, *Nature*, 460, 213
- Cattaneo A., Woo J., Dekel A., Faber S. M., 2013, *MNRAS*, 430, 686
- Ceverino D., Dekel A., Bournaud F., 2010, *MNRAS*, 404, 2151
- Ceverino D., Dekel A., Mandelker N., Bournaud F., Burkert A., Genzel R., Primack J., 2012, *MNRAS*, 421, 2151
- Chang Y.-Y., van der Wel A., Rix H.-W., Holden B., Bell E. F., McGrath E. J., Wuyts S., et al., 2013, *ApJ*, 773, 149
- Cheung E. et al., 2012, *ApJ*, 760, 131
- Ciotti L., Ostriker J. P., 2007, *astro-ph/0703057*
- Codis S., Pichon C., Devriendt J., Slyz A., Pogosyan D., Dubois Y., Sousbie T., 2012, *MNRAS*, 427, 3320
- Crocker A., Krips M., Bureau M., Young L. M., Davis T. A., Bayet E., Alatalo K., et al., 2012, *MNRAS*, 421, 1298
- Daddi E. et al., 2010, *ApJ*, 713, 686
- Damjanov I., Abraham R. G., Glazebrook K., McCarthy P. J., Caris E., Carlberg R. G., Chen H.-W., et al., 2011, *ApJ*, 739, L44
- Damjanov I., McCarthy P. J., Abraham R. G., Glazebrook K., Yan H., Mentuch E., Le Borgne D., et al., 2009, *ApJ*, 695, 101
- Danovich M., Dekel A., Hahn O., Teyssier R., 2012, *MNRAS*, 422, 1732
- Dekel A., Birnboim Y., 2006, *MNRAS*, 368, 2
- Dekel A., Birnboim Y., 2008, *MNRAS*, 383, 119
- Dekel A. et al., 2009, *Nature*, 457, 451
- Dekel A., Krumholz M. R., 2013, *MNRAS*, 432, 455
- Dekel A., Sari R., Ceverino D., 2009, *ApJ*, 703, 785
- Dekel A., Silk J., 1986, *ApJ*, 303, 39
- Dekel A., Zolotov A., Tweed D., Cacciato M., Ceverino D., Primack J. R., 2013, *MNRAS*, 435, 999
- Dutton A. A., van den Bosch F. C., Dekel A., Courteau S., 2007, *ApJ*, 654, 27
- El-Zant A. A., Kim W.-T., Kamionkowski M., 2004, *MNRAS*, 354, 169
- Elmegreen B. G., Burkert A., 2010, *ApJ*, 712, 294

- Elmegreen B. G., Zhang H.-X., Hunter D. A., 2012, *ApJ*, 747, 105
- Elmegreen D. M., Elmegreen B. G., Ferguson T. E., 2005, *ApJ*, 623, L71
- Emsellem E., Cappellari M., Krajnović D., Alatalo K., Blitz L., Bois M., Bournaud F., et al., 2011, *MNRAS*, 414, 888
- Fabian A. C., 2012, *ARA&A*, 50, 455
- Fall S. M., Efstathiou G., 1980, *MNRAS*, 193, 189
- Fang J. J., Faber S. M., Koo D. C., Dekel A., 2013, *ApJ*, 776, 63
- Forbes J., Krumholz M., Burkert A., 2012, *ApJ*, 754, 48
- Forbes J. C., Krumholz M. R., Burkert A., Dekel A., 2013, *arXiv:1305.2925*
- Forster Schreiber N. M. et al., 2009, *ApJ*, 706, 1364
- Gabor J. M., Bournaud F., 2013, *MNRAS*, 434, 606
- Gammie C. F., 2001, *ApJ*, 553, 174
- Genel S., Dekel A., Cacciato M., 2012, *MNRAS*, 425, 788
- Genel S. et al., 2012, *ApJ*, 745, 11
- Genzel R. et al., 2008, *ApJ*, 687, 59
- Genzel R., Förster Schreiber N. M., Lang P., Tacchella S., Tacconi L. J., Wuyts S., et al., 2013, *arXiv:1310.3838*
- Genzel R., Newman S., Jones T., Förster Schreiber N. M., Shapiro K., Genel S., Lilly S. J., et al., 2011, *ApJ*, 733, 101
- Genzel R., Tacconi L. J., Eisenhauer F., Förster Schreiber N. M., Cimatti A., Daddi E., Bouché N., et al., 2006, *Nature*, 442, 786
- Hopkins P. F., Hernquist L., Cox T. J., Robertson B., Springel V., 2006, *ApJS*, 163, 50
- Hopkins P. F., Kereš D., Murray N., Quataert E., Hernquist L., 2012, *MNRAS*, 427, 968
- Hopkins P. F., Quataert E., Murray N., 2012, *MNRAS*, 421, 3522
- Immeli A., Samland M., Gerhard O., Westera P., 2004a, *A&A*, 413, 547
- Immeli A., Samland M., Westera P., Gerhard O., 2004b, *ApJ*, 611, 20
- Kannappan S. J., 2004, *ApJ*, 611, L89
- Kauffmann G., Li C., Fu J., Saintonge A., Catinella B., Tacconi L. J., Kramer C., et al., 2012, *MNRAS*, 422, 997
- Kaviraj S. et al., 2013a, *MNRAS*, 428, 925
- Kaviraj S. et al., 2013b, *MNRAS*, 429, L40
- Kereš D., Katz N., Fardal M., Davé R., Weinberg D. H., 2009, *MNRAS*, 395, 160
- Kereš D., Katz N., Weinberg D. H., Davé R., 2005, *MNRAS*, 363, 2
- Khochfar S., Ostriker J. P., 2008, *ApJ*, 680, 54
- Kimm T., Devriendt J., Slyz A., Pichon C., Kassin S. A., Dubois Y., 2011, *arXiv:1106.0538*
- Krumholz M. R., Burkert A., 2010, *ApJ*, 724, 895
- Krumholz M. R., Dekel A., 2010, *MNRAS*, 406, 112
- Krumholz M. R., Dekel A., 2012, *ApJ*, 753, 16
- Krumholz M. R., Dekel A., McKee C. F., 2012, *ApJ*, 745, 69
- Krumholz M. R., Thompson T. A., 2013, *MNRAS*, 434, 2329
- Larson R. B., 1976, *MNRAS*, 176, 31
- Law D. R., Steidel C. C., Shapley A. E., Nagy S. R., Reddy N. A., Erb D. K., 2012, *ApJ*, 759, 29
- Lee B., Giallisco M., Williams C. C., Guo Y., Lotz J., Van der Wel A., Ferguson H. C., et al., 2013, *ApJ*, 774, 47
- Mac Low M.-M., 1999, *ApJ*, 524, 169
- Maller A. H., Dekel A., 2002, *MNRAS*, 335, 487
- Martig M., Bournaud F., Teyssier R., Dekel A., 2009, *ApJ*, 707, 250
- Martig M., Crocker A. F., Bournaud F., Emsellem E., Gabor J. M., Alatalo K., Blitz L., et al., 2013, *MNRAS*, 432, 1914
- Mihos J. C., Hernquist L., 1996, *ApJ*, 464, 641
- Mo H. J., Mao S., White S. D. M., 1998, *MNRAS*, 295, 319
- Murray N., Quataert E., Thompson T. A., 2005, *ApJ*, 618, 569
- Murray N., Quataert E., Thompson T. A., 2010, *ApJ*, 709, 191
- Neistein E., Dekel A., 2008, *MNRAS*, 388, 1792
- Neistein E., van den Bosch F. C., Dekel A., 2006, *MNRAS*, 372, 933
- Nelson D., Vogelsberger M., Genel S., Sijacki D., Kereš D., Springel V., Hernquist L., 2013, *MNRAS*, 429, 3353
- Newman A. B., Ellis R. S., Treu T., Bundy K., 2010, *ApJ*, 717, L103
- Newman S. F. et al., 2013, *ApJ*, 767, 104
- Noguchi M., 1999, *ApJ*, 514, 77
- Ocvirk P., Pichon C., Teyssier R., 2008, *MNRAS*, 390, 1326
- Pichon C., Pogosyan D., Kimm T., Slyz A., Devriendt J., Dubois Y., 2011, *MNRAS*, 418, 2493
- Saintonge A., Tacconi L. J., Fabello S., Wang J., Catinella B., Genzel R., Graciá-Carpio J., et al., 2012, *ApJ*, 758, 73
- Stewart K. R., Brooks A. M., Bullock J. S., Maller A. H., Diemand J., Wadsley J., Moustakas L. A., 2013, *ApJ*, 769, 74
- Tacconi L. J. et al., 2010, *Nature*, 463, 781
- Tacconi L. J., Neri R., Genzel R., Combes F., Bolatto A., Cooper M. C., Wuyts S., et al., 2013, *ApJ*, 768, 74
- Tillson H., Devriendt J., Slyz A., Miller L., Pichon C., 2012, *arXiv:1211.3124*
- Toomre A., 1964, *ApJ*, 139, 1217
- van der Wel A. et al., 2011, *ApJ*, 730, 38
- van Dokkum P. G. et al., 2008, *ApJ*, 677, L5
- van Dokkum P. G., Kriek M., Franx M., 2009, *Nature*, 460, 717
- Whitaker K. E., Kriek M., van Dokkum P. G., Bezanon R., Brammer G., Franx M., Labbé I., 2012, *ApJ*, 745, 179
- Williams C. C. et al., 2013, *arXiv:1310.3819*